Active Flow Control of Low-Pressure Turbine by Dielectric Barrier Discharge Plasma Actuator

L. Yue, Y.F. Wang*, X.Z. Ma,
X. Zhao and Y.W. Zhang

School of Transportation and Vehicle Engineering, Shandong University of Technology, No. 266 Xincun West Road, 255049, Zibo, China

Received: 14.01.2022 & Accepted: 26.04.2022

Doi: 10.12693/APhysPolA.142.233 *e-mail: wangyunfei@sdut.edu.cn

In order to reduce dynamic loss and improve the performance of low-pressure turbines, the technology of active flow control of a dielectric barrier discharge plasma actuator was used to control the internal flow of a low-pressure turbine using a numerical simulation method. In this paper, the effect of plasma actuation on the cascade flow field with different actuator positions and applied voltages was studied. The results show that the closer the plasma actuator is to the leading edge of the cascade, the better the control effect of the plasma actuation. When the actuator is aligned with the leading edge of the cascade, the total pressure loss at the outlet is reduced by 4.5%. Plasma actuation has a greater ability to restrain outlet loss at higher voltage, but the control effect tends to saturation as the applied voltage increases. Total pressure loss is reduced by 8.2% for $U_0 = 15$ kV. The plasma actuation decreases the lateral pressure gradient in the cascade passage thus suppresses the lateral movement of low energy fluids from the pressure side to the suction side. The height of the passage vortex and total pressure loss are restrained, which is an important reason for decreasing outlet loss.

topics: low-pressure turbine, dielectric barrier discharge plasma, total pressure loss, passage vortex

1. Introduction

The aeroengine is the heart of the aircraft and it is of great importance in terms of the national security strategy. In order to improve the efficiency of thermal cycle and unit thrust of the engine, high efficiency, low maintenance cost, and other design technologies are commonly used in turbines [1, 2]. However, when the aircraft cruises at high altitude, the Reynolds number decreases sharply due to the significant reduction of air density. Especially in the case of high-load low-pressure turbines, the internal lateral pressure gradient and the reverse pressure are stronger. Profile loss and secondary flow loss are aggravated, the aerodynamic performance of low-pressure turbines deteriorates. Therefore, the complex flow in low-pressure turbines has always attracted great attention of researchers [3–5].

Marks et al. [6–8] carried out many experimental studies on losses of high-load low-pressure turbines. The results showed that boundary layer separation affects the performance of a low-pressure turbine at a low Reynolds number. As the Reynolds number decreases, the total pressure loss will increase rapidly due to the separation of the boundary layer. In addition, incoming turbulence also affects the separation and transition process of the boundary layer and the total pressure loss. The lower the Reynolds number, the more likely the boundary layer separation will occur. This would change the flow state of the boundary layer on the suction surface and further affect the blade profile loss and secondary flow loss.

To reduce the total pressure loss and restrain boundary layer separation, researchers are using active and passive control methods to control the internal flow of low-pressure turbines. However, passive control cannot match all the working conditions of a low-pressure turbine. Changing the working conditions of low-pressure turbines often produces unnecessary losses. Some active flow control techniques, such as air suction, steady jet blowing, and pulsed jet blowing, overcome the shortcomings of passive flow control. On the other hand, they probably bring more additional weight and make the engine structure more complex. Dielectric barrier discharge (DBD) plasma actuation is a new active flow control technology based on plasma aerodynamic actuation, which is mainly used to reduce the drag of supersonic vehicles.

In recent decades, research of discharge plasma has gradually developed. Audier et al. [9, 10] described the variation of ionic wind with time, and the dynamics when the discharge is switched on.

They found that breakdown streamers play an important role in the ionic wind hydrodynamics. Due to the existence of breakdown streamers, the frequency of the pulsed ionic produced by the positive corona discharge corresponds to the frequency of the current pulses. Bartnik et al. [11] investigated the effect of low-temperature plasma induced by extreme ultraviolet on surface modification. The results showed that the molecular structure of the exposed material is modified under the dual action of radiation pulses and low temperature plasma. Babij et al. [12] studied the application of the atmospheric pressure plasma on mass spectrometry. They showed that the atmospheric pressure plasma has many advantage over low pressure plasma in various aspects, and that the cold plasma is of great promise in application (industry, medicine, biology). Pereira et al. [13, 14] carried out experiments to study the identifying cross-talk effects between DBD plasma actuators that are arranged in the boundary layer and the external flow. The results showed that the power consumption did not change with the flow velocity. However, as the free stream velocities increase, the plasma light emission tends to increase in intensity. Based on induced actuator perturbation, a methodology was provided [13, 14] to derive a local frequency response of flow when the actuator is turned on. In order to study the power characteristics of surface dielectric barrier discharge, Xu et al. [15, 16] developed a physics-based SDBD power model that can be used to accurately calculate the power of actuators of various geometries and materials. Many experiments have been carried out by these authors in which it was demonstrated that the DBD enhanced electroaerodynamic (EAD) propulsion device has lower power consumption and can increase the endurance of EAD aircraft. Im et al. [17, 18] studied the effect of a turbulent boundary layer actuation in a supersonic flow. The results showed that the actuation effect of the turbulent boundary layer obviously makes the boundary layer thinner. Matsunuma et al. [19] applied discharge plasma to control tip clearance leakage flow. The mechanism of plasma control of leakage flow has been found to improve the axial momentum of tip clearance flow. The plasma actuation also has a good effect on reducing the boundary layer drag. Mahfoze et al. [20] used the plasma actuator to generate a jet to control a coherent structure in a turbulent boundary layer, and the drag was reduced by 33.5%. The plasma actuation is also used to control boundary layer separation. Zhang et al. [21] used large eddy simulation (LES) to study the control effect of plasma actuation on boundary layer flow. It was found that plasma actuation located in the boundary layer can induce a small-scale spanwise vortex in the flow field, which developed downstream driven by the mainstream to form the wall jet. It could restrain the flow mixing in the turbulent boundary layer and reduce the total pressure loss in the boundary layer. Pescini et al. [22, 23] made curved wall profiles to simulate the suction surface of low-pressure turbine blades on a flat plate and carried out many experiments on the effect of plasma actuation on the boundary layer separation. The results showed that the reverse pressure area along the curved wall is separated without actuation. In addition, there was a large area of high turbulent kinetic energy at the junction of the mainstream and the separated area. The plasma actuation reduced the extension of the separation area and the magnitude of negative flow velocity.

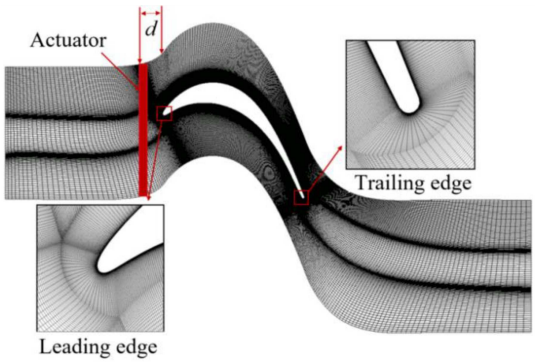

Fig. 1. Grid for the computational domain.

As a new active flow control technology, dielectric barrier discharge plasma actuation flow control overcomes the drawbacks of passive flow control. This technology has been applied in many fields due to its simple structure, quick reaction, and low energy consumption. In this paper, plasma actuation is applied to control the internal flow of a low-pressure turbine. The optimal position of the plasma actuator was selected through numerical simulation. At the optimal position, the effect of plasma actuation with different applied voltage on the cascade flow field was investigated. The mechanism of plasma actuation on the internal flow of a low-pressure turbine is shown. It enriches the flow control theory aimed to reduce the dynamic loss and provide a theoretical basis for the optimization of low-pressure turbines.

2. Numerical simulation method

In this paper, Fig. 1 shows the grid distribution of the end wall of the T106A cascade and a magnification of the grid around the leading edge and trailing edge. The red part of the figure shows the position of the plasma actuator. All cases use the same grid, the inlet boundary is $1.0C_{ax}$ from the leading edge of the cascade (C_{ax} is the axial chord length), and the outlet boundary is $1.4C_{ax}$ from the trailing edge of the cascade. Since the flow field structures of the upper and lower half of the cascade are nearly symmetrical, it is assumed that the boundary condition of $50\%H$ (H is the blade height) section is symmetry. The lower half of the cascade is selected as the

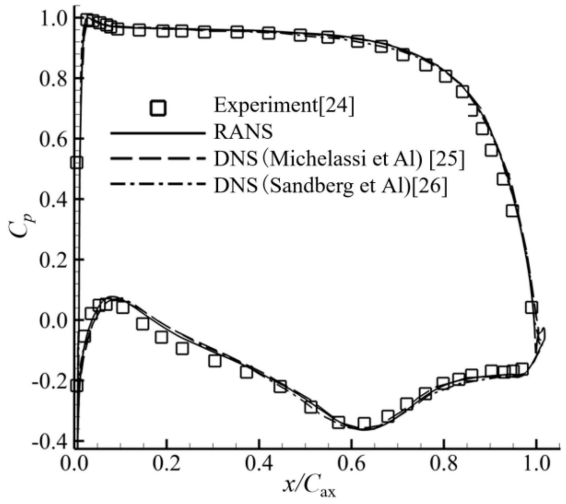

Fig. 2. Static pressure coefficient at 50%H.

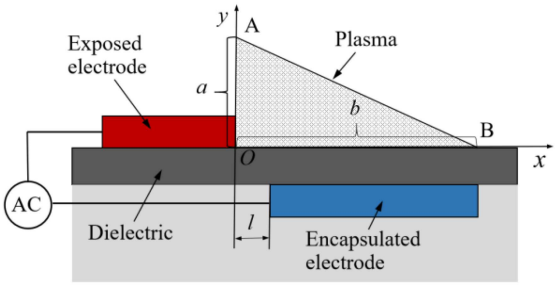

Fig. 3. Phenomenological model of the plasma actuator.

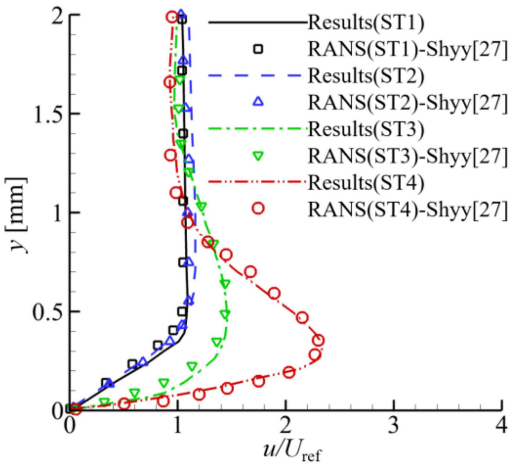

Fig. 4. The induced velocity of plasma actuation at different positions.

computational domain. In order to get more details of the flow field and to improve the calculation accuracy, 127 nodes are arranged in the circumferential direction, 938 nodes in the flow direction, and 100 nodes in the spanwise direction. The grid number of the whole computational domain is about 4 million.

It is assumed that the inflow conditions of all considered cases are the same. The Reynolds numbers (Re_{2th}) of all cases are outlet Reynolds numbers according to the isentropic expansion process, thus $\mathrm{Re}_{2th} = 0.6 \times 10^5$. The outlet Mach number is $\mathrm{Ma}_2 = 0.4$. The inlet turbulence is set to 0.5%. It can be assumed that the relative velocity between the wall and the air flow on the wall is zero, so the boundary condition of the cascade surface and the end wall are assumed to be non-slip walls. The calculation results are compared with the experimental [24] and direct numerical simulation (DNS) [25, 26] data. The static pressure coefficient of the cascade can directly reflect the pressure distribution and is an important parameter to study the evolution of the boundary layer. The distribution of the static pressure coefficient on the surface of the cascade at 50%H (H is the cascade height) is shown in Fig. 2. The static pressure coefficient is defined as

$$C_p = \frac{p - p_2}{p_{t1} - p_2}. \tag{1}$$

Here, p is the static pressure on the cascade surface, p_{t1} is the total pressure at the inlet, p_2 is the static pressure at the outlet. From the data comparison, it can be seen that the calculated results are in good agreement with the experimental data and the DNS data.

The phenomenological model of the plasma actuator is shown in Fig. 3. Two electrodes are arranged asymmetrically, i.e., one is exposed to air and the other is encapsulated in an insulating medium. When the applied voltage is higher than the breakdown threshold, the air between the two electrode plates will be ionized. Since the duration of this process is very short, around a few nanoseconds, it can be assumed that when the plasma actuator is turned on, the action of plasma will be generated immediately. According to the theory of Shyy et al. [27], ignoring the chemical reaction and the electric field force, the action of plasma is simplified as the volume force. The inductive effect is to move the surrounding air to the side of the encapsulated electrode, forming a wall jet. It is assumed that the volume force exists only in the region of OAB. The electric field strength at the O point is $E_0 = U_0/l$, U_0 is the maximum voltage applied between the two electrodes, and $l = 0.25$ mm. The electric field strength decreases linearly with increasing distance from O point, and the electric field strength in the OAB region is $E = E_0 - k_1 x - k_2 y$. The breakdown threshold of the electric field strength is $E_b = 30$ kV/cm, the electric field strength in the directions x and y, respectively, is as follows

$$E_x = \frac{k_2}{\sqrt{k_1^2 + k_2^2}} E \tag{2}$$

and

$$E_y = \frac{k_1}{\sqrt{k_1^2 + k_2^2}} E. \tag{3}$$

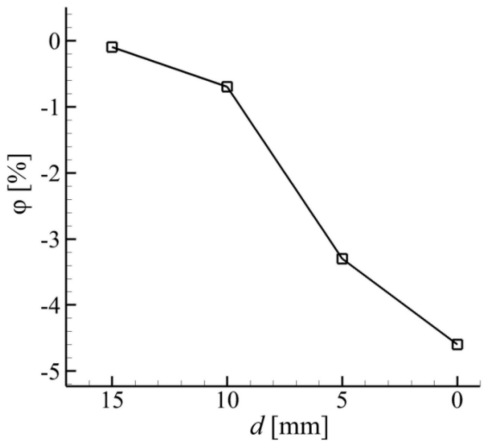

Fig. 5. Change rate of the average total pressure loss at the outlet.

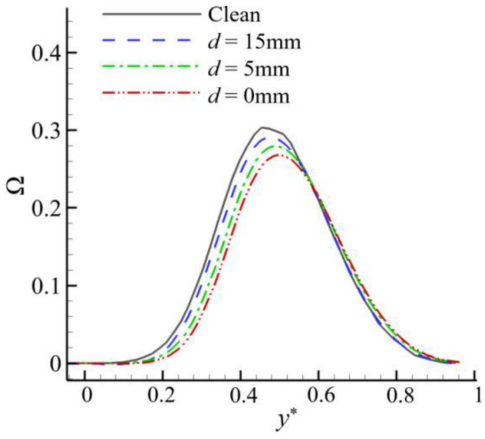

Fig. 6. Distribution of total pressure loss coefficient at the outlet 50%H along the circumferential direction.

Here, $k_1 = (E_0 - E_b)/b$, $k_2 = (E_0 - E_b)/a$, $a = 0.0015$ m, $b = 0.003$ m. Thus, the volume force components of the electric field in x and y directions are, respectively,

$$F_x = \rho_e e E_x f \, \Delta t \tag{4}$$

and

$$F_y = \rho_e e E_y f \Delta t. \tag{5}$$

Here, f is the power frequency, e is the elementary charge, and the electron number density is $\rho_e = 1 \times 10^{17}$ m^{-3}. The plasma discharge time in the excitation cycle of AC power is $\Delta t = 67$ μs.

Figure 4 shows the induced velocity of plasma actuation at various positions. The plasma-induced flow field results with the incoming flow of 5 m/s and the loading voltage of 5 kV are compared to those given by Shyy [27] (U_{ref} is the velocity of the incoming flow). As can be seen in Fig. 4, the induction velocity and disturbance range of this model are in good agreement with the results given in [27]. Therefore, the accuracy of the phenomenological model has been verified.

3. Effects of plasma actuation with different actuator positions on the cascade end wall

In order to determine the optimal position of the plasma actuator upstream of the cascade, the effect of plasma actuation at different positions when the applied voltage is 5 kV is studied. the installation distance between the actuator and the leading edge of the cascade is d. The plasma actuator is aligned with the leading edge of the cascade when $d = 0$. Figure 5 shows the change rate of the average total pressure loss (φ) at the outlet.

Figure 6 shows the distribution of the spanwise average total pressure loss coefficient (Ω) at the outlet of the cascade along the circumferential direction. This coefficient is defined as

$$\Omega = \frac{p_{t1} - p_{t2}}{p_{t1} - p_2}. \tag{6}$$

Here, p_{t2} is the local total pressure. The circumferential dimension is normalized based on the pitchwise direction size. The pressure side is represented by $y^* = 0$ and the suction side is represented by $y^* = 1$.

As can be seen in Fig. 5, the total pressure loss at the outlet reduced under the influence of the plasma actuation. The change rate of the total pressure loss is inversely proportional to the installation distance. This means that as the installation distance decreases, the total pressure loss at the outlet decreases as well. When the actuator is aligned with the leading edge of the cascade, the change rate of the total pressure loss at the outlet is 4.5%. Figure 6 shows the distribution of the total pressure loss coefficient at the outlet 50%H along the circumferential direction. The phenomenon shown in Fig. 6 is generally consistent with Fig. 5. In the cases of plasma actuation, the total pressure loss decreases along the major circumferential direction. The peak value of the total pressure loss coefficient appears near $y^* = 0.45$, the effect of plasma actuation is more significant in this position. When the actuator is aligned with the leading edge of the cascade, the peak total pressure loss coefficient is reduced by 16.7%. In addition, the change of the peak point is also very obvious. As the installation distance decreases, the peak point gradually moves towards the suction side. The position of the whole loss curve also moves with it. It is inferred that under the condition of low Reynolds number, the plasma actuation changes the outlet airflow angle. Thus, it additionally affected the loss area distribution of the cascade flow field. In conclusion, the closer the actuator is to the leading edge of the cascade, the better the control effect of plasma actuation is. Therefore, it is necessary to continue the research at $d = 0$. In the following, the actuate intensity of the actuation will be adjusted by changing the applied voltage, and the effect of plasma actuation with different applied voltages at the position of $d = 0$ on the cascade flow field will be studied.

4. Effects of plasma actuation with different applied voltage

Figure 7 shows the static pressure coefficient of the cascade surface under different applied voltages when the plasma is aligned with the leading edge of the cascade. It can be seen at $5\%H$ in Fig. 7a that the static pressure coefficient in the front half of the suction surface decreases in a small range in the case of plasma actuation. The greater the applied voltage is, the greater the decrease is. The reason for this phenomenon is that the actuator injects more momentum into the air, making it difficult for low-energy air to gather here, resulting in a decrease in the static pressure coefficient. In the rear half of the suction surface, the static pressure coefficient increases to different degree in the range of 0.55–$0.85C_{ax}$. The higher the applied voltage is, the larger the static pressure coefficient is. The reduction of the lateral pressure between the blades can effectively restrain the secondary flow movement in the cascade passage. With the applied voltage increasing from 0 to 15 kV, the maximum variation of the static pressure coefficient is 27%. After $0.85C_{ax}$, the static pressure coefficient of the suction surface with actuation is smaller than that without actuation, but the discrepancy of actuation effect under different applied voltage is reduced.

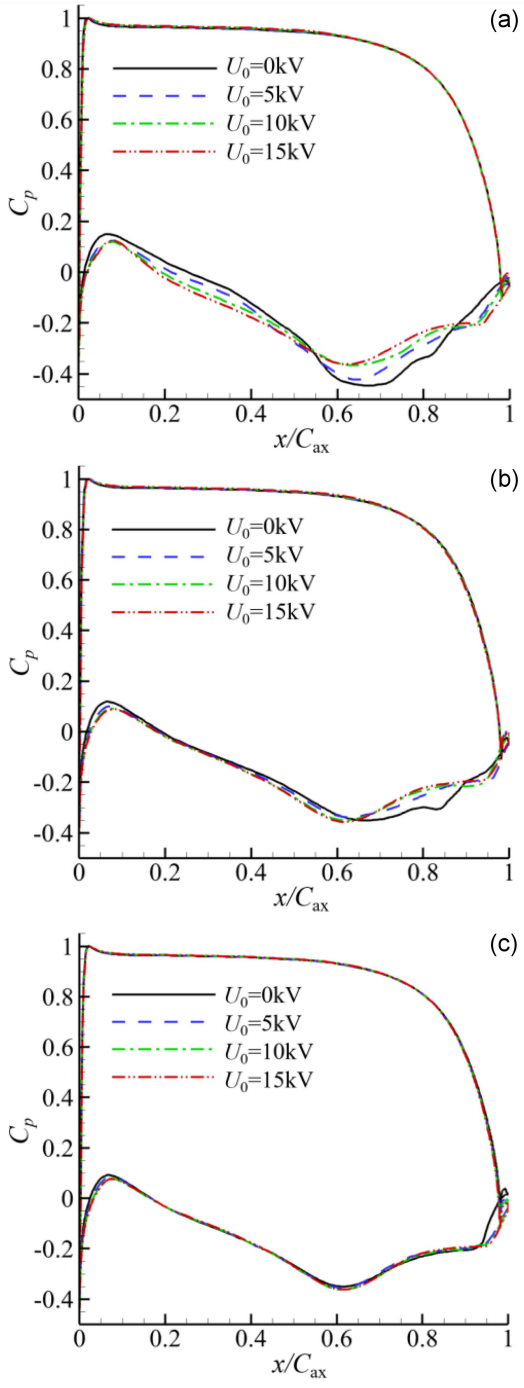

Fig. 7. Static pressure coefficient of cascade surface under different applied voltage, i.e., (a) $5\%H$, (b) $10\%H$, (c) $20\%H$.

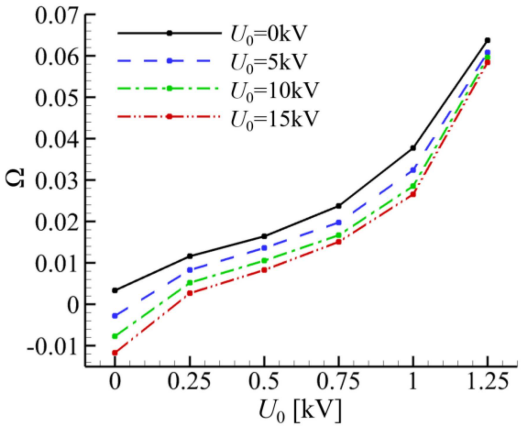

Fig. 8. Average total pressure loss coefficient at different streamwise positions.

In Fig. 7b, the plasma actuation mainly affects the pressure at the rear of the suction surface at $10\%H$. The actuation effect is very weak in the region above $10\%H$. The cascade surface pressure does not change with the exception for the area near the trailing edge. It is inferred that the influence of plasma actuation on the pressure distribution is mainly concentrated in the region below $10\%H$. The actuation effect on the pressure surface is very weak. The increase of the static pressure coefficient of the suction side reduces the lateral pressure in the cascade passage, thus restraining the lateral movement of the passage vortex from the pressure side to the suction side. Moreover, it suppresses the intensity of the secondary flow in the end region and reduces the total pressure loss of the cascade.

The average total pressure loss coefficient at various streamwise positions and the change rate of the average total pressure loss with different applied voltages at the outlet are shown in Figs. 8 and 9, respectively. The total pressure loss decreases from the leading edge to $1.25C_{ax}$ of the cascade with the increase of applied voltages (see Fig. 8). At any

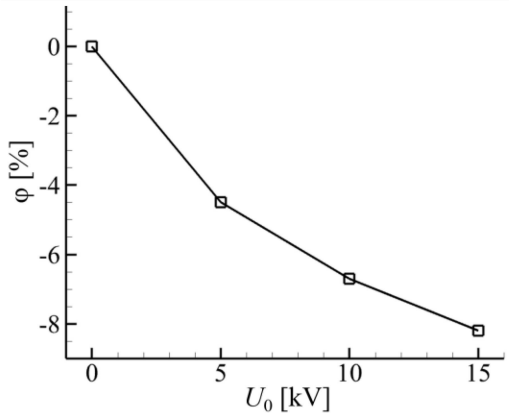

Fig. 9. Change rate of the average total pressure loss with different applied voltages at the outlet.

streamwise position, the larger the applied voltage is, the larger the amplitude of total pressure loss reduction. The discrepancy of the total pressure loss reduction in different cases gradually reduces with the increase of the applied voltages. However, at different streamwise positions, the magnitude of total pressure loss reduction decreases along the streamwise direction. Up to the outlet, as shown in Fig. 9, the total pressure loss is reduced by 8.2% in the case of $U_0 = 15$ kV. The plasma actuation has a strong ability to restrain the outlet loss, but the control effect tends to saturation at higher applied voltage.

The circumferential average total pressure loss coefficient at $1.0C_{ax}$ section and the outlet along the spanwise direction in the cases of different applied voltages are shown in Fig. 10. The total pressure loss coefficient below $8\%H$ is reduced due to the plasma actuation on the end wall (see Fig. 10a). The peak point of total pressure loss in all cases locates in the range of 8–$14\%H$. The plasma actuation changes the location of the peak point of total pressure loss so that it is closer to the end wall. After the air flows from the trailing edge to the outlet, the location of the peak point of total pressure loss rises continuously. But peak value of the total pressure loss decreases. It indicates that the intensity of the passage vortex keeps weakening as it develops downstream of the cascade. The plasma actuation has a strong reduction effect on the total pressure loss (see Fig. 10b). At the case of $U_0 = 5$ kV, the passage vortex loss area is obviously divided into two smaller loss areas. The trend of loss reduction has begun to emerge. With the increase of the applied voltage, the two small loss areas are combined again. But the total pressure loss in this area is lower than that without plasma actuation.

The total pressure loss coefficient at different heights of the outlet along the circumferential direction is shown in Fig. 11. In Fig. 11(a) and b, the peak value of the total pressure loss increases slightly in the cases of plasma actuation below $10\%H$. This means that the plasma actuation does

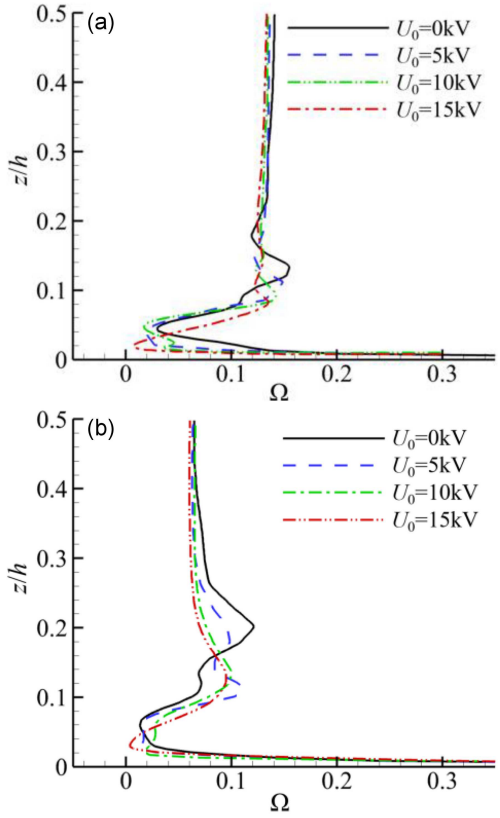

Fig. 10. Circumferential average total pressure loss coefficient on different flow direction sections, i.e., (a) $100\%C_{ax}$ (b) outlet.

not reduce the total pressure loss anywhere in the flow field. In turn, in Fig. 11c and d, the plasma actuation has a positive control effect on the flow field above $20\%H$. The peak value of the total pressure loss was greatly reduced and decreased nonlinearly with the increase of the applied voltage at $20\%H$. The maximum reduction is 25% in the case of $U_0 = 15$ kV. The total pressure loss at the outlet increases at first and then decreases along the spanwise direction. The total pressure loss is higher at $20\%H$, and the effect of plasma actuation is also stronger near this region, which significantly reduces the peak value of total pressure loss. Note that the location of the peak point of the total pressure loss is closer to the suction side. It can be inferred that the outlet flow angle is changed by plasma actuation, the wake downstream of the cascade moves to the suction side. In addition, although the plasma actuation increases the total pressure loss below $10\%H$, it has a positive control effect in other larger areas (above $20\%H$). As shown in Fig. 9, the average total pressure loss at the outlet is significantly reduced.

The total pressure loss coefficients at different streamwise sections under different applied voltages are given in Fig. 12. Starting from the leading edge of the cascade, under the action of lateral pressure in the cascade passage, the pressure side leg

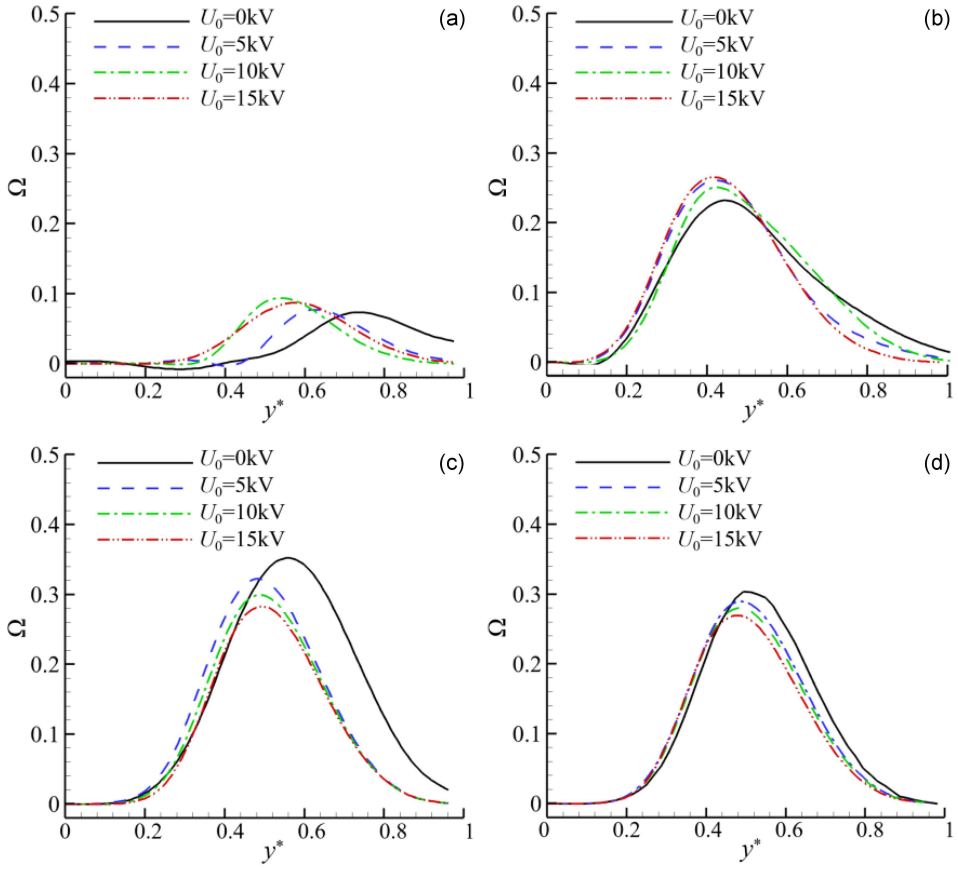

Fig. 11. Total pressure loss coefficient at different heights of the outlet along the circumferential direction, i.e., (a) 5%H, (b) 10%H, (c) 20%H, (d) 50%H.

of the horseshoe vortex moves to the suction side and the trailing edge of the cascade. In the process of flow, more and more low-energy fluid gathers towards the corner region of the suction side. At the 50%C_{ax} position, the fluid reached the suction surface and rolled up. It then converges with the suction side leg of the horseshoe vortex, forming a passage vortex. Then, the passage vortex rises and expands along the streamwise direction, the area of the high loss region also increases. In the cases of plasma actuation, the area of the high loss region near the leading edge is greatly reduced, so that the intensity of the pressure side leg of the horseshoe vortex is obviously restrained. In addition, the reduction of the lateral pressure in the cascade passage was also taken into account, the intensity of the passage vortex was suppressed.

It should be noted that the high loss region near the boundary layer at the back of the suction surface extends towards the end wall with the weakening of the passage vortex (see Fig. 12m–p). Nevertheless, as shown in Fig. 9, the average total pressure loss on the entire section decreases compared to the case without plasma actuation.

The three-dimensional streamlines of the end zone and limit streamlines of the cascade are given in Fig. 13. In Fig. 13a and b, some low energy air with a greater viscosity of the air at a low Reynolds number is attached to the end wall. The suction side leg of the horseshoe vortex rises rapidly after entering the cascade passage. It then converges with the pressure side leg of horseshoe vortex, forming a strong passage vortex. With the involvement of more low-energy air, the passage vortex continues to grow along the streamwise direction. The three-dimensional separation of suction surface inflow and separation bubbles appears at SL_1. There is a strong interference between the passage vortex and the separation bubble at the rear of the suction surface which restrains the extending of recirculation region to the end wall. At the same time, the existence of the separation bubble also blocks the passage vortex from climbing upward (at SL_2). In Fig. 13c and d, the suction side leg of the horseshoe vortex rises slightly after entering the cascade passage, so that the height of the passage vortex decreases. The separation lines SL_1 and SL_2 move to the end wall. According to the analysis above, the intensity of the passage vortex and total pressure loss are reduced. In addition, with the weakening of the passage vortex, the interference between the passage vortex and the separation bubble becomes weaker. The recirculation region reappears between the passage vortex and the suction surface.

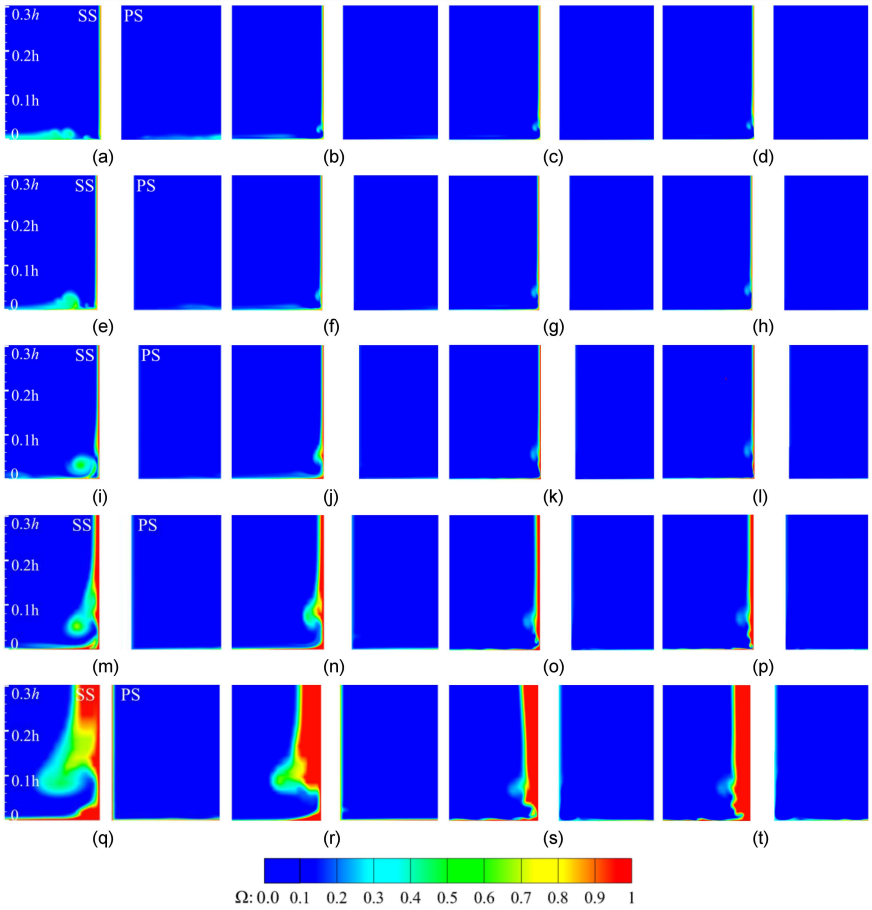

Fig. 12. The total pressure loss coefficients at different flow direction sections, i.e., (a) clean, 10%C_{ax}, (b) 5 kV, 10%C_{ax}, (c) 10 kV, 10%C_{ax}, (d) 15 kV, 10%C_{ax}, (e) clean, 25%C_{ax}, (f) 5 kV, 25%C_{ax}, (g) 10 kV, 25%C_{ax}, (h) 15 kV, 25%C_{ax}, (i) clean, 50%C_{ax}, (j) 5 kV, 50%C_{ax}, (k) 10 kV, 50%C_{ax}, (l) 15 kV, 50%C_{ax}, (m) clean, 75%C_{ax}, (n) 5 kV, 75%C_{ax}, (o) 10 kV, 75%C_{ax}, (p) 15 kV, 75%C_{ax}, (q) clean, 100%C_{ax}, (r) 5 kV, 100%C_{ax}, (s) 10 kV, 100%C_{ax}, (t) 15 kV, 100%C_{ax}.

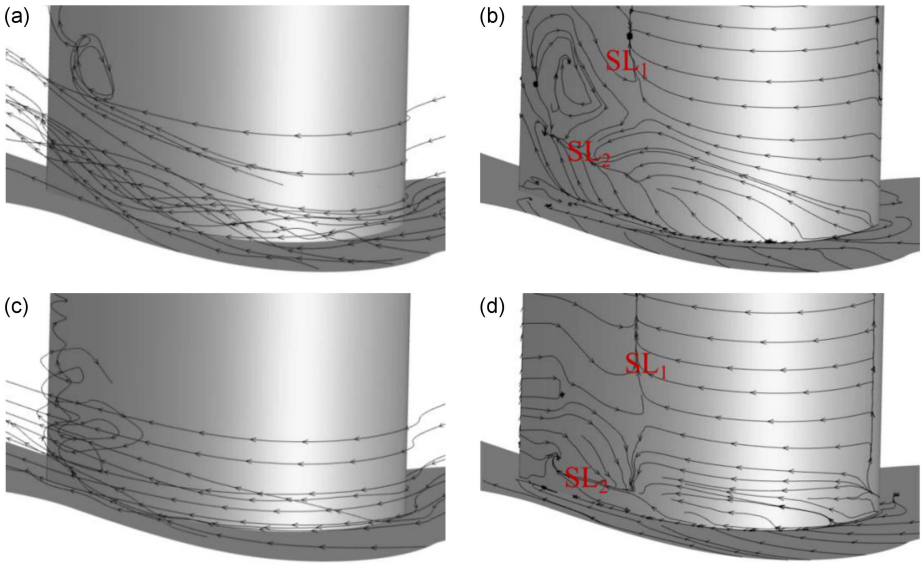

Fig. 13. Three-dimensional streamline of the end area and limit streamline of the suction surface. (a) Three-dimensional streamline of the end area, 0 kV. (b) The limit streamline of the suction surface, 0 kV. (c) Three-dimensional streamline of the end area, 15 kV. (d) Limit streamline of the suction surface, 15 kV.

5. Conclusion

In this paper, a three-dimensional computational domain model and a transition SST turbulence model are adopted. The effect of plasma actuation on the cascade flow field at different actuator positions and applied voltages was studied. The results show that

1. The closer the plasma actuator is to the leading edge of the cascade, the better the control effect of the plasma actuation. When the actuator is aligned with the leading edge of the cascade, the total pressure loss at the outlet is reduced by 4.5%.
2. Plasma actuation has a stronger ability to restrain the outlet loss at higher voltage, but the control effect tends to saturate when the applied voltage increases. The total pressure loss is reduced by 8.2% in the case of $U_0 = 15$ kV.
3. Plasma actuation decreases the lateral pressure gradient in the cascade passage, thus suppressing the lateral movement of low-energy fluids from the pressure side to the suction side. The height of the passage vortex and the total pressure loss are restrained, which is an important reason for the decrease of outlet loss.

Acknowledgments

This work was supported by the project ZR2020QE190 supported by Shandong Provincial Natural Science Foundation and The National Natural Science Foundation of China (No. 51906243).

References

[1] R.J. Goldstein, R.A. Spores, *ASME J. Heat Transfer.* **110**, 862 (1988).

[2] Y.F. Wang, H.L. Chen, H.P. Liu, Y.P. Song, F. Chen, *Proc. Inst. Mech. Eng. Part G J. Aerosp. Eng.* **235**, 1187 (2021).

[3] T. Schubert, S. Chemnitz, R. Niehuis, *J. Turbomach.* **143**, 1 (2021).

[4] A.P. Duben, T.K. Kozubskaya, O.V. Marakueva, D.V. Voroshnin, *J. Phys. Conf. Ser.* **1891**, 012018 (2021).

[5] S. Sun, T.R. Tan, X.S. Wu, L. Meng, H.L. Du, A.W. Shen, *Tuijin Jishu/J. Propuls. Technol.* **42**, 2474 (2021).

[6] A. Gross, C.R. Marks, R. Sondergaard, P.S. Bear, J.M. Wolff, *J. Propuls. Power.* **34**, 27 (2018).

[7] M.H. Donovan, M.P. Rumpfkeil, C.R. Marks, N. Fletcher, in: *AIAA Scitech 2021 Forum*, 2021 p. 1.

[8] P. Bear, M. Wolff, A. Gross, C.R. Marks, R. Sondergaard, *ASME. J. Turbomach.* **140**, 031003 (2018).

[9] P. Audier, M. Fénot, N. Bénard, E. Moreau, *Appl. Phys. Lett.* **108**, 084103 (2016).

[10] E. Moreau, P. Audier, T. Orriere, *J. Appl. Phys.* **125**, 133303 (2019).

[11] A. Bartnik, H. Fiedorowicz, W. Skrzeczanowski, J. Czwartos, P. Wachulak, R. Jarocki, J. Kostecki, *Acta Phys. Pol.* **133**, 267 (2018).

[12] M. Babija, T. Gotszalka, Z.W. Kowalskia, K. Nitscha, J. Silberringb, M. Smoluch, *Acta Phys. Pol.* **125**, 1260 (2014).

[13] R. Pereira, D. Ragni, M. Kotsonis, *J. Appl. Phys.* **116**, 103301 (2014).

[14] R. Pereira, M. Kotsonis, G.D. Oliveira, D. Ragni, *J. Appl. Phys.* **118**, 153301(2015).

[15] H.F. Xu, Y. He, S.R.H. Barrett, *Appl. Phys. Lett.* **114**, 254105 (2019).

[16] N.D. Wilde, H.F. Xu, N. Gomez-Vega, S.R.H. Barrett, *Appl. Phys. Lett.* **118**, 154102 (2021).

[17] S. Im, M.A. Cappelli, *Appl. Phys. Lett.* **100**, 264103 (2012).

[18] S. Im, H. Do, M.A. Cappelli, *Appl. Phys. Lett.* **97**, 041503 (2010).

[19] T. Matsunuma, T. Segawa, in: *ASME Turbo Expo 2018*, ASME Paper No. GT2018-76680 (2018).

[20] O. Mahfoze, S. Laizet, *Int. J. Heat Fluid Flow* **66**, 83 (2017).

[21] H.D. Zhang, Y. Wu, Y.H. Li, *Int. J. Heat Fluid Flow* **80**, 108502 (2019).

[22] E. Pescini, A. Suma, M. G. De Giorgi, A. Francioso, A. Ficarella, *Energy Procedia* **126**, 786(2017).

[23] E. Pescini, M.G. De Giorgi, A. Suma, A. Francioso, A. Ficarella, *Aerosp. Sci. Technol.* **76**, 442(2018).

[24] P. Stadtmüller, "Investigation of Wake-Induced Transition on the LP Turbine Cascade T106A-EIZ", DFG-Verbundproject Fo 136/11, Ver. 1.0 (2001).

[25] V. Michelassi, L.W. Chen, R. Pichler, R.D. Sandberg, *J. Turbomach.* **137**, 071005 (2015).

[26] R.D. Sandberg, R. Pichler, L. Chen, in: *13th International Symposium for Unsteady Aerodynamics, Aeroacoustics and Aeroelasticity in Turbomachinery (ISUAAAT)*, 2012.

[27] W. Shyy, B. Jayaraman, A. Andersson, *J. Appl. Phys.* **92**, 6434 (2002).